

ADVANCED MATERIALS

Supporting Information

for *Adv. Mater.*, DOI: 10.1002/adma.201603601

Probing Bilayer Grain Boundaries in Large-Area Graphene
with Tip-Enhanced Raman Spectroscopy

*Kyoung-Duck Park, Markus B. Raschke, Joanna M. Atkin,
Young Hee Lee, and Mun Seok Jeong**

Supporting Information to: Probing Bilayer Grain Boundaries in Large Area Graphene with Tip-Enhanced Raman Spectroscopy

Kyoung-Duck Park,¹ Markus B. Raschke,¹ Joanna M.

Atkin,² Young Hee Lee,^{3,4} and Mun Seok Jeong^{3,4}

¹*Department of Physics, Department of Chemistry, and JILA, University of Colorado, Boulder, CO, 80309, United States*

²*Department of Chemistry, University of North Carolina, Chapel Hill, North Carolina 27599, United States*

³*Center for Integrated Nanostructure Physics, Institute for Basic Science, Sungkyunkwan University, Suwon 440-746, Republic of Korea*

⁴*Department of Energy Science, Sungkyunkwan University, Suwon 440-746, Republic of Korea*

(Dated: September 29, 2016)

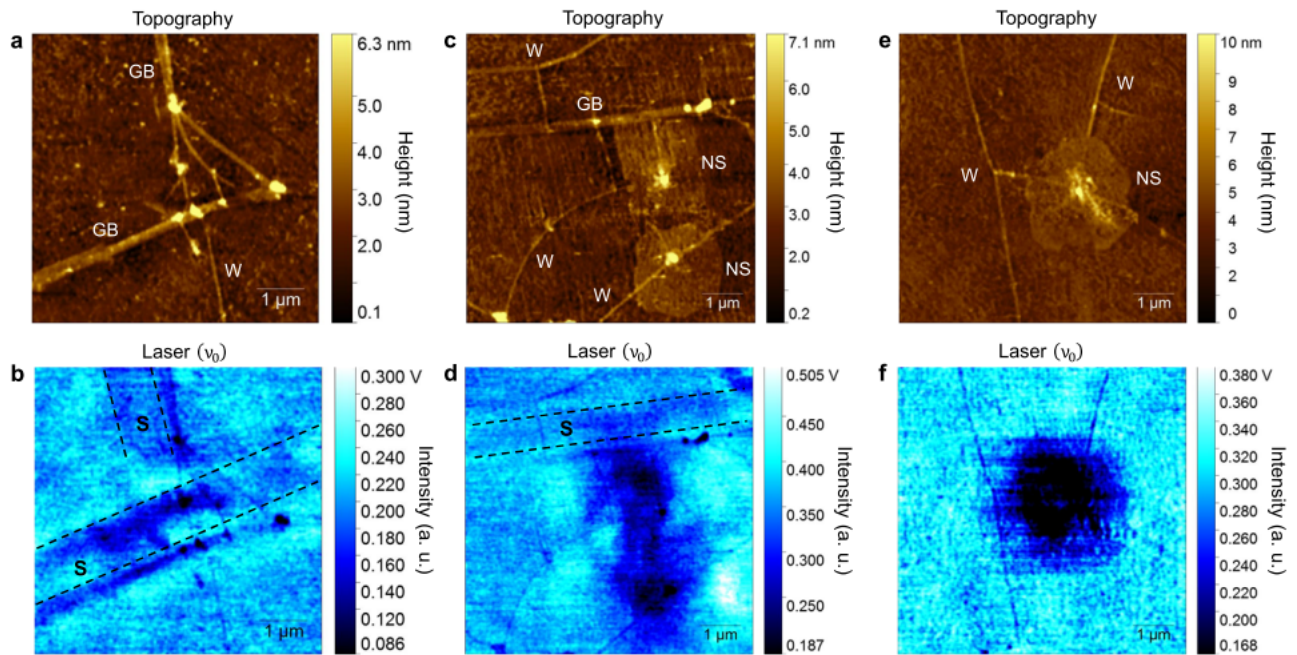


Figure S1. (a, c, e) Topographies of CVD grown large area graphene measured by shear force AFM exhibiting wrinkle (W) and grain boundary (GB) structures. (b, d, f) Simultaneously measured tip-enhanced Rayleigh scattering images.

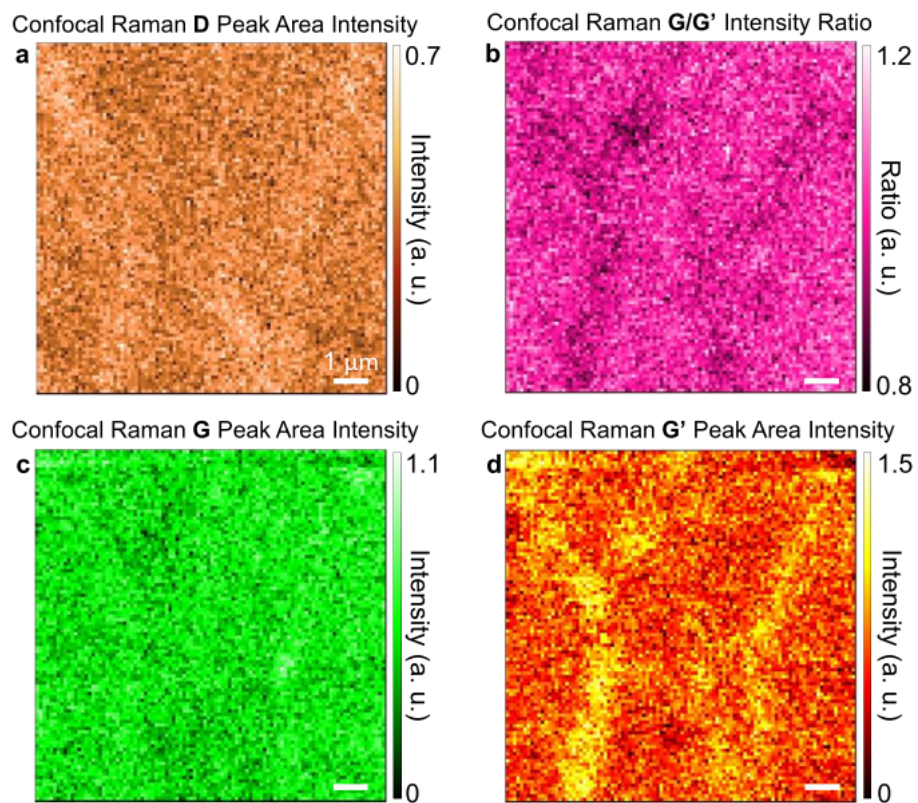


Figure S2. Confocal Raman images of D peak area intensity (a), G/G' intensity ratio (b), G peak area intensity (c), and G' peak area intensity (d) are derived from multispectral confocal Raman imaging (0.5 s acquisition times per pixel). This measurement is performed as same condition as Fig. 2 of the main text after retracting the Au tip from sample.

CLASSIFICATION OF THE WRINKLES, GRAIN BOUNDARIES, AND FOLDED STRUCTURES

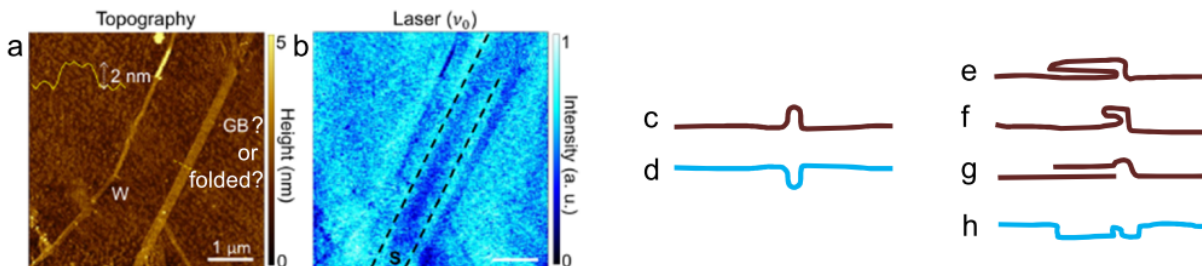


Figure S3. (a) Topography of a CVD grown large area graphene measured by shear force AFM exhibiting line defects. (b) Simultaneously measured tip-enhanced Rayleigh scattering image. Expected cross-sections of the wrinkle structures (c), and its optical signal (d). Expected cross-sections of the folded or grain boundary structures (e-g), and optical signal (h) for the structures (e) and (g).

For type classification of the line defects in large area graphene, we consider four analysis stages: (1) Topographic feature (AFM), (2) Expected cross-section, (3) Optical feature, (4) Raman feature.

1. Confirmation of the wrinkles

- (1) Topographic feature (AFM): narrow width (~ 50 nm).
- (2) Expected cross-section: from the measured AFM image, we can infer the cross-section of the wrinkle similar to Fig. S3c.
- (3) Optical feature: from the expected cross-sectional structure, we can infer the cross-section of the optical image similar to Fig. S3d, which could be observed due to stronger absorption compared to the monolayer crystal face. Fig. S3d is also in good agreement with the measured near-field scattering image (Fig. S3b).
- (4) Raman feature: the G' peak intensity should be decreased due to the structural curvature effect with no change in D and G peaks (see Fig. 4).

\Rightarrow From these correlated analysis, we classify the wrinkle from various line defects.

2. Confirmation of the other line defects: grain boundary (GB) and folded

- (1) Topographic feature (AFM): wide width (~ 200 nm).
- (2) Expected cross-section: from the measured AFM image, we can infer the cross-section of both the folded structures such as Fig. S3e and f and grain boundary structure such as Fig. S3g. The folded structures should be trilayer with AB or 0° (near 0°) stacking angles. While the grain boundary should be bilayer with random stacking angles.
- (3) Optical feature: from the measured near-field scattering image (Fig. S3b) similar to Fig. S3h, we can exclude the possibility of the expected cross-section (f).
- (4) Raman feature:
- a) Folded (Fig. S3e): for AB trilayer graphene, according to the group theory analysis, fifteen Raman G' peaks are allowed since there are multiple electron-phonon scatterings from K to K' point which occurred by three different iTO phonon branches [1]. Experimentally, the FWHM of AB trilayer graphene should be clearly broader than monolayer graphene with asymmetric spectral shape, and also the G' peak intensity should be weaker than monolayer [1]. Raman properties of the 0° (near 0°) stacking angle trilayer graphene should also be similar to AB trilayer graphene.
 - b) Grain boundary (Fig. S3g): from the bilayer with random misorientation angles, various combinations of Raman D, G, and G' peaks should be observed. Therefore, the line defects in Fig. 2 of the main text are bilayer grain boundaries.
- \Rightarrow From these correlated analysis, we classify the grain boundaries and folded structures from various line defects.

ANALYSIS OF OTHER AREA AND OBSERVATION OF FOLDED STRUCTURE

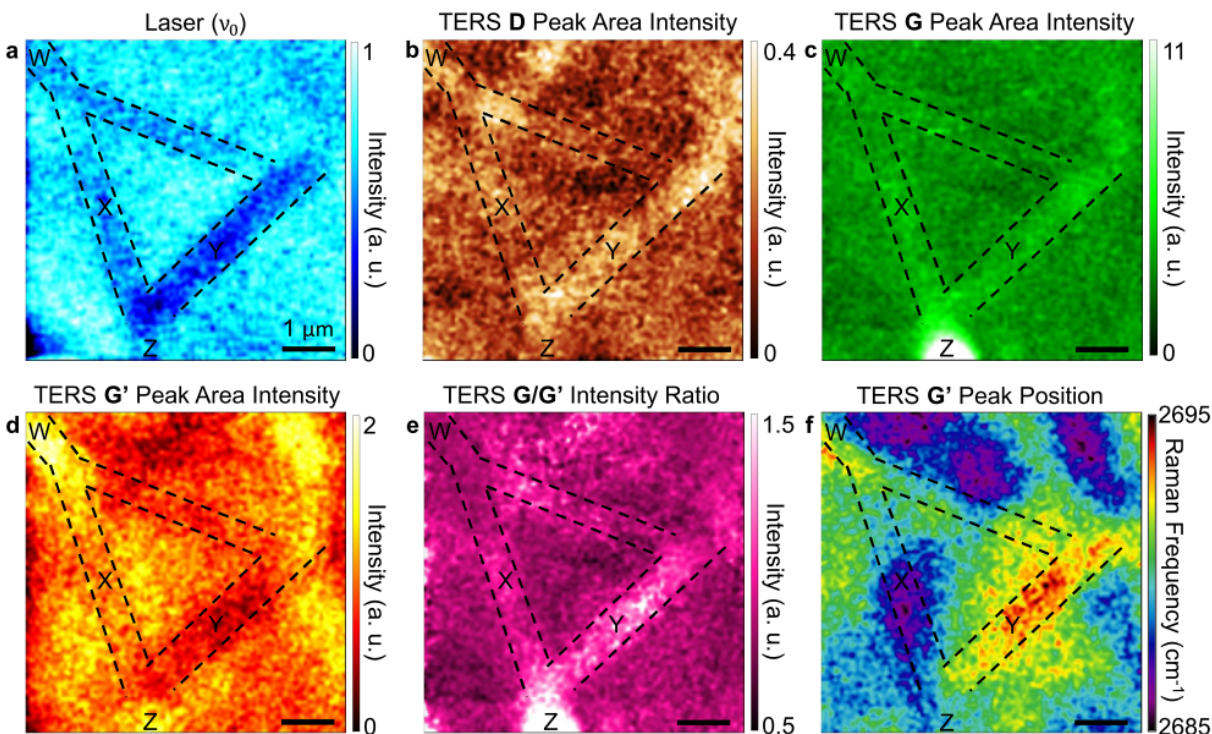


Figure S4. (a) Tip-enhanced Rayleigh scattering image of a CVD grown graphene exhibiting line defects such as grain boundaries and folded structure. Tip-enhanced Raman D peak area intensity (b), G peak area intensity (c), G' peak area intensity (d), TERS images of G/G' intensity ratio (e), and peak position of G' peak are derived from multispectral TERS imaging (0.2 s acquisition time per pixel).

Fig. S4a-f show the near-field Rayleigh scattering image and TERS responses, which reveal structural properties of line defects observed in CVD-grown large area graphene. The distinguishable line structures from the near-field Rayleigh scattering image are indicated by black dashed lines in the TERS images (Fig. S4b-f). As we explained in the main text, the dark regions in the near-field scattering image are feature of the multilayer graphene due to the stronger absorption than monolayer regions. TERS images of D, G, and G' peaks show distinct Raman response at various line defects, labeled W, X, Y, and Z. In the case of the line W, the G' peak is stronger in intensity and slightly blueshifted in spectral position compared to monolayer region. In contrast, for the line X, the G' peak intensity is comparable to monolayer region while the G peak intensity is increased. From these features,

we can classify the line W and X as bilayer grain boundaries, and estimate the misorientation angles ($W > 13^\circ$, $X < 5^\circ$) as we explained the detailed analysis method in the main text. The misorientation angle of indicated bilayer region Z is easily interpreted as $\sim 10^\circ$ since the G peak intensity is strongly increased only near the critical angle θ_c . Interestingly, the line defect Y shows decreased G' peak intensity with evidently more increased G peak intensity than bilayer GBs. These features cannot be explained by the theoretical vibrational properties of the twisted stacking bilayer graphene [2]. In addition, from the near-field Rayleigh scattering image (Fig. S4a), we find that absorption in line defect Y is clearly stronger than bilayer GBs. This feature means the line Y is possibly the folded structure of monolayer since it should be a trilayer. Further, the blueshifted Raman frequency of the G' peak (Fig. S4f) also supports this hypothesis.

ANALYSIS OF ADDITIONAL LINE DEFECTS IN FIG. 2

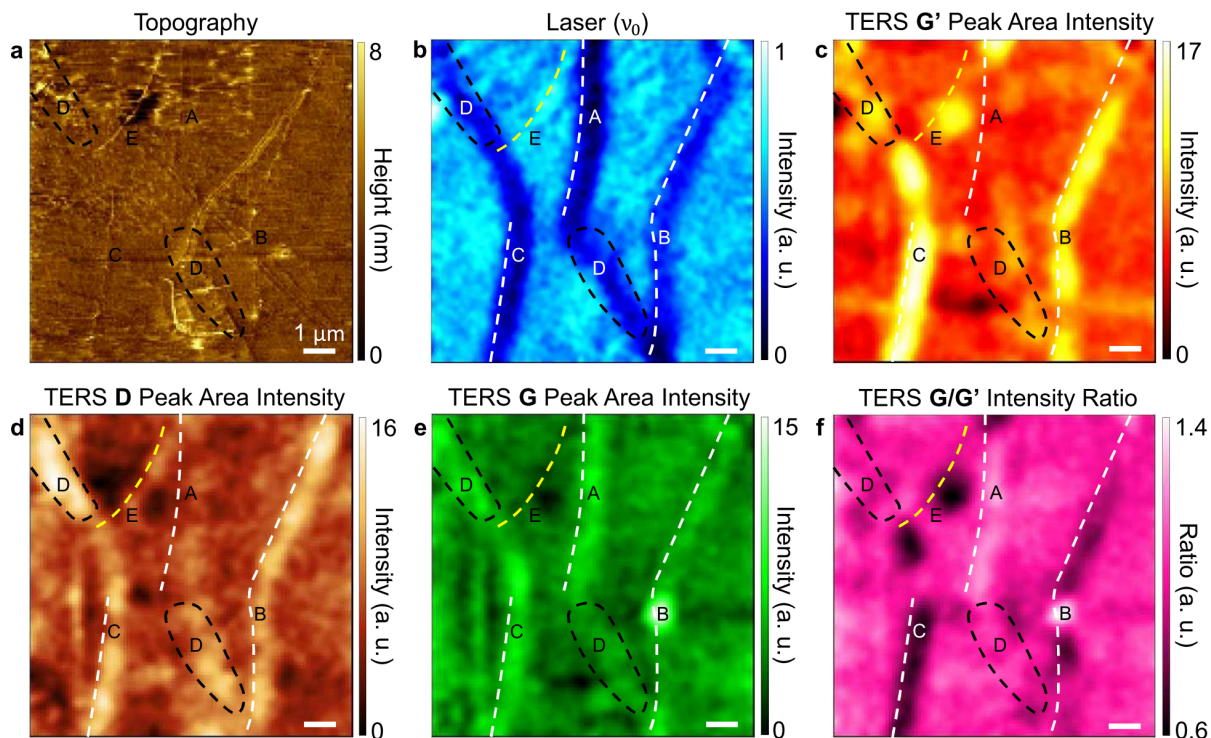


Figure S5. (a) Topography of a CVD grown graphene exhibiting structural defects such as wrinkles and grain boundaries. (b) Tip-enhanced Rayleigh scattering image. G' peak area intensity (c), D peak area intensity (d), G peak area intensity (e), and TERS images of G/G' intensity ratio (f) are derived from multispectral TERS imaging (0.5 s acquisition time per pixel), measured simultaneously with (a) and (b).

Structural properties of A, B, and C (indicated by white dashed lines) revealed from correlated analysis are explained in the main text. In case of the GBs in regions D (indicated by black dashed lines), the G peak is slightly stronger in intensity compared to monolayer with the comparable intensity of the G' peak, whereas the D peak intensity is remarkably increased in the overall regions D. Therefore, the GBs in the regions D are bilayer structures with small misorientation angles. However, the TERS properties of G and G' peaks are not clearly measured due to the surface contaminants, which cause intensity increase of the D peak. From the topography (a), we confirm the surface contaminants in these regions, which are not observed in the regions of A, B, and C. On the other hand, the line defect E is interpreted as a non-carbon defects on the monolayer crystal surface since intensities of

the near-field scattering and the Raman D peak are increased with the slightly decreased G peak intensity. Intensity decrease of the G peak cannot be observed in any cases for the multilayer graphene.

THE ORIGIN OF WRINKLES

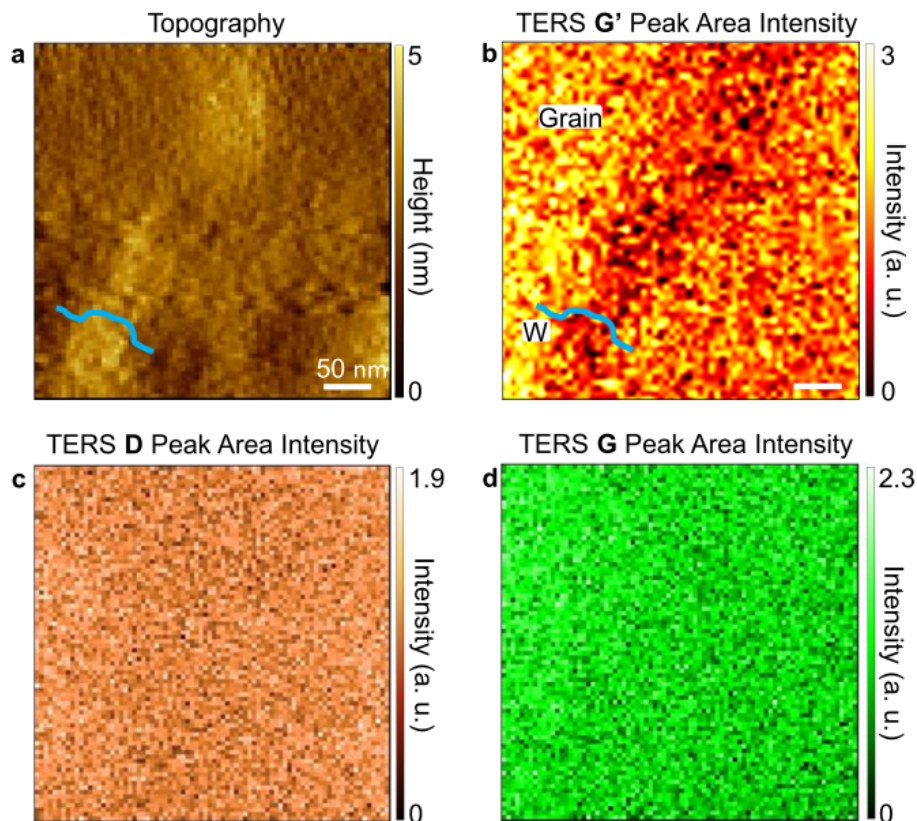


Figure S6. (a) Topography of wrinkle structure. Simultaneously measured TERS images of G' peak area intensity (b), D peak area intensity (c), and G peak area intensity (d).

The wrinkles are mainly formed in the CVD growth process due to the thermal expansion coefficient difference between underlying substrate (Cu or Ni) and graphene [3, 4]. A small percentage of the wrinkles could be formed during the transfer process which show distinguishing feature of bi-wrinkle formation [4]. Our group have also demonstrated the detailed studies of the origin of wrinkles in the CVD process in previous studies [5, 6]. Since we have used the graphene sample using same CVD growth condition as those references and also not observed the bi-wrinkle formation, we believe the wrinkle we measured was created in the growth process.

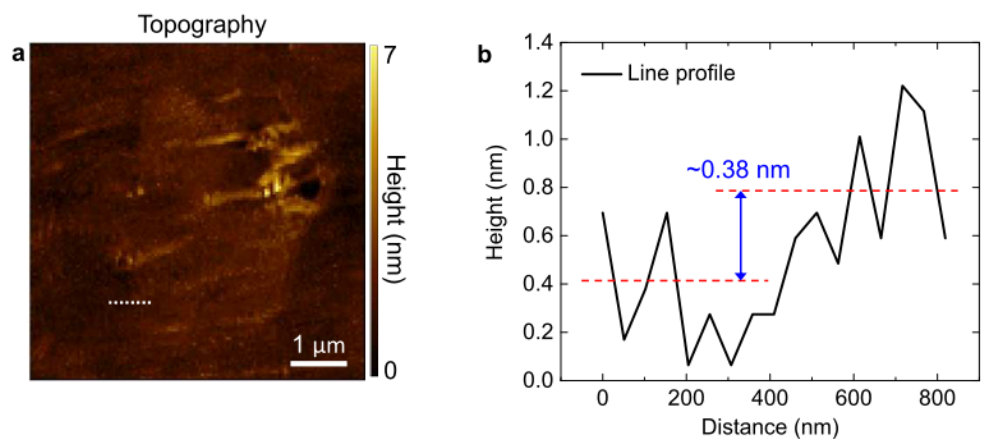


Figure S7. (a) Topography of nucleation site. Simultaneously measured near-field scattering and TERS images are shown in the main text. (b) Line profile at the boundary of bilayer seed and monolayer graphene indicated by white dashed line in the topography (a). Monolayer thickness of graphene (~ 0.35 nm) is roughly confirmed despite the vertical resolution of a shear-force AFM is ~ 1 nm.

-
- [1] Malard, L., Pimenta, M., Dresselhaus, G. & Dresselhaus, M. Raman spectroscopy in graphene. *Physics Reports* **473**, 51–87 (2009).
- [2] Coh, S., Tan, L. Z., Louie, S. G. & Cohen, M. L. Theory of the raman spectrum of rotated double-layer graphene. *Physical Review B* **88**, 165431 (2013).
- [3] Li, X. *et al.* Large-area synthesis of high-quality and uniform graphene films on copper foils. *Science* **324**, 1312–1314 (2009).
- [4] Liu, N. *et al.* The origin of wrinkles on transferred graphene. *Nano Research* **4**, 996–1004 (2011).
- [5] Chae, S. J. *et al.* Synthesis of large-area graphene layers on poly-nickel substrate by chemical vapor deposition: wrinkle formation. *Advanced Materials* **21**, 2328–2333 (2009).
- [6] Han, G. H. *et al.* Influence of copper morphology in forming nucleation seeds for graphene growth. *Nano Letters* **11**, 4144–4148 (2011).